Inorganic Chemistry

Article

pubs.acs.org/IC

Photo- and Vapor-Controlled Luminescence of Rhombic Dicopper(I) Complexes Containing Dimethyl Sulfoxide

Atsushi Kobayashi,[†] Kahori Komatsu,[†] Hiroki Ohara,[†] Waka Kamada,[†] Yuko Chishina,[†] Kiyoshi Tsuge,[‡] Ho-Chol Chang,[§] and Masako Kato*[,†]

[†]Department of Chemistry, Faculty of Science, Hokkaido University, North-10 West-8, Kita-ku, Sapporo 060-0810, Japan

[‡]Department of Chemistry, Graduate School of Science and Engineering, University of Toyama, Toyama 930-8555, Japan

[§]Department of Applied Chemistry, Faculty of Science and Engineering, Chuo University, 1-13-27, Kasuga, Bunkyo-ku, Tokyo 112-8551, Japan

Supporting Information

ABSTRACT: Halide-bridged rhombic dicopper(I) complexes, $[Cu_2(\mu\text{-}X)_2(DMSO)_2(PPh_3)_2]$ (X = I^-, Br^-; DMSO = dimethyl sulfoxide; PPh_3 = triphenylphosphine), were synthesized, the iodide complex of which exhibited interesting photochromic luminescence driven by photoirradiation and by exposure to DMSO vapor in the solid state. Single-crystal X-ray diffraction measurements revealed that the iodo and bromo complexes (abbreviated **Cu_2I_2-[O,O]** and **Cu_2Br_2-[O,O]**) were isomorphous, and that the two DMSO ligands were coordinated to the Cu(I) ion via the O atom in both complexes. Both complexes exhibited bright blue phosphorescence at room temperature (λ_{em} = 435 nm, Φ_{em} = 0.19 and 0.14 for **Cu_2I_2-[O,O]** and **Cu_2Br_2-[O,O]**, respectively) with a relatively long emission lifetime ($\tau_{em} \sim 200$ μs at 77 K) derived from the mixed halide-to-ligand and metal-to-ligand charge transfer (^{3}XLCT and ^{3}MLCT) excited state. Under UV irradiation, the blue phosphorescence of **Cu_2Br_2-[O,O]** disappeared uneventfully and no new emission band appeared, whereas the blue phosphorescence of **Cu_2I_2-[O,O]** rapidly disappeared with simultaneous appearance of a new green emission band (λ_{em} = 500 nm). On further irradiation, the green emission of the iodide complex gradually changed to bright yellowish-green (λ_{em} = 540 nm); however, this change could be completely suppressed by lowering the temperature to 263 K or in the presence of saturated DMSO vapor. The initial blue phosphorescence of **Cu_2I_2-[O,O]** was recovered by exposure to DMSO vapor at 90 °C for a few hours. IR spectroscopy and theoretical calculations suggest that the DMSO ligand underwent linkage isomerization from O-coordination to S-coordination, and both the occurrence of linkage isomerization and the removal of DMSO result in contraction of the rhombic $Cu_2(\mu\text{-}I)_2$ core to make the Cu···Cu interaction more effective. In the contracted core, the triplet cluster-centered (^{3}CC) emissive state is easily generated by thermal excitation of the ^{3}XLCT and ^{3}MLCT mixed transition state, resulting in the green to yellowish-green emission. In contrast, the Cu···Cu distance in **Cu_2Br_2-[O,O]** is considerably longer than that of **Cu_2I_2-[O,O]**, which destabilizes the ^{3}CC emissive state, resulting in the nonemissive character.

INTRODUCTION

The strong emission, colorful luminescence, oxygen gas sensing capabilities, etc. of luminescent Cu(I) complexes continues to capture the interest of researchers.[1−3] These emissive Cu(I) complexes are emerging candidates for the construction of phosphorescent materials for organic light-emitting devices (OLEDs) from inexpensive, abundant, nonprecious metal complexes.[4−6] Among the many phosphorescent or delayed-fluorescent Cu(I) complexes reported thus far,[7−14] halide-bridged tetranuclear Cu(I) cluster complexes have been extensively studied.[15−22] The tetranuclear cubane-type Cu(I) cluster complexes $[Cu_4I_4(PPh_3)_4]$ and $[Cu_4I_4py_4]$ (PPh_3 = triphenylphosphine, py = pyridine) exhibit strong phosphorescence originating from triplet cluster-centered (^{3}CC) and/or triplet metal-to-ligand charge transfer (^{3}MLCT) transition states,[19,22] and some of them also exhibit interesting thermochromic luminescence originating from the temperature-dependent metallophilic (Cu···Cu) interaction in the tetranuclear cluster core.[21,22] These Cu(I) cluster complexes are also attractive as prospective luminescent molecular building blocks.[23−28] Braga et al. recently reported interesting vapochromic luminescence from a metal−organic framework built from iodide-bridged cubane-type tetranuclear Cu_4I_4 cores with a bridging organic linker, $[Cu_4I_4(DABCO)_2]$ (DABCO = 1,4-diazabicyclo[2,2,2]octane).[25] Despite the abundance of luminescent Cu(I) cluster complexes reported to date, few of them exhibit photochromic behavior.

The linkage isomerization reactions of ambidentate ligands, such as NO, SO_2, SCN^-, and DMSO (DMSO = dimethyl

Received: August 21, 2013
Published: November 4, 2013

   dx.doi.org/10.1021/ic402104q | Inorg. Chem. 2013, 52, 13188−13198

sulfoxide), have been exploited by us and other researchers recently, because some of these isomerization reactions can be driven by photoirradiation.[29−40] For example, Rack and coworkers reported several Ru(II)− and Os(II)−DMSO complexes that exhibit interesting photochromic behavior based on the photoinduced linkage isomerization from the S-coordinated isomer to the O-coordinated counterpart.[36−38] However, these photochromic Ru(II)−DMSO complexes were not luminescent, in contrast with the bright phosphorescence observed for many Ru(II)−polypyridine complexes (e.g., $[Ru(bpy)_3]^{2+}$ (bpy = 2,2′-bipyridine)),[41] possibly because the photochromic behavior generally originates from photoinduced structural conversion (e.g., *cis*−*trans* isomerization of azobenzene), which competes with the luminescence process. To achieve simultaneous photochromism and luminescence, the halide-bridged dicopper(I) rhombic core was selected as both the luminophore and the coordinating site for the DMSO ligand given that the large difference between the coordination geometries of Cu(I) and Cu(II) ions may provide a moderate activation barrier to control the linkage isomerization reaction of DMSO in the photoexcited state. Herein, we report the syntheses, crystal structures, and luminescence properties of halide-bridged rhombic dicopper(I) complexes, $[Cu_2(\mu\text{-}X)_2(DMSO)_2(PPh_3)_2]$, (X = I^-, Br^-; PPh_3 = triphenylphosphine; DMSO = dimethyl sulfoxide) bearing a typical ambidentate DMSO ligand, and demonstrate that the luminescence color of the iodide complex is dramatically influenced by photoinduced and thermally assisted linkage isomerization, and release and readsorption of the DMSO ligand.

EXPERIMENTAL SECTION

General Procedures. All commercially available starting materials were used as received, and solvents were used without purification. Unless otherwise stated, all manipulations were conducted in air. The ^{1}H NMR spectrum of each sample was measured using a JEOL EX-270 NMR spectrometer at room temperature. Elemental analysis was conducted at the analysis center at Hokkaido University.

Synthesis of $[Cu_2(\mu\text{-}I)_2(DMSO)_2(PPh_3)_2]$ (Cu_2I_2-[O,O]). A 10 mL portion of PPh_3 (117.1 mg, 0.446 mmol) in DMSO was added to a DMSO solution (10 mL) of CuI (85.1 mg, 0.446 mmol). After storage for 1 day at 293 K, colorless block crystals emerged. These crystals were collected by filtration, washed with acetone, and dried in air. Yield: 144.9 mg, 61.4%. Elemental analysis calculated for $C_{40}H_{42}Cu_2I_2O_2P_2S_2$: C 45.25, H 3.99, S 6.04, I 23.90; found C 45.10, H 3.82, S 6.15, I 23.48. ^{1}H NMR ($CDCl_3$, 298 K): δ 7.53 (t, 12H), 7.41−7.26 (m, 18 H), 2.62 (s, 12H). IR (KBr, cm^{-1}): 3052 m, 3000 m, 2910 w, 1585 w, 1478 s, 1433 s, 1396 m, 1307 m, 1286 w, 1181 w, 1158 w, 1095 s, 1028 s, 1021 s, 1002 s, 946 s, 934 m, 854 w, 743 s, 694 s, 619 w, 519 s, 502 s, 498 w, 436 m.

Synthesis of $[Cu_2(\mu\text{-}Br)_2(DMSO)_2(PPh_3)_2]$ (Cu_2Br_2-[O,O]). The bromide complex **Cu_2Br_2-[O,O]** was obtained through a similar synthetic method as that used for **Cu_2I_2-[O,O]** by replacing CuI with CuBr. Yield: 171.8 mg, 79.6%. Elemental analysis calculated for $C_{40}H_{42}Cu_2Br_2O_2P_2S_2$: C 49.64, H 4.37, S 6.63, Br 16.51; found C 49.58, H 4.21, S 6.61, Br 16.75. ^{1}H NMR ($CDCl_3$, 298 K): δ 7.52 (t, 12H), 7.26−7.40 (m, 18H), 2.62 (s, 12H). IR (KBr, cm^{-1}): 3043 m, 2999 m, 2908 w, 1478 s, 1435 s, 1399 m, 1308 m, 1287 w, 1182 w, 1160 w, 1095 s, 1023 s, 1005 s, 948 s, 937 m, 854 w, 743 s, 695 s, 618 w, 519 s, 498 w, 436 m.

Single-Crystal X-ray Diffraction Measurements. All single-crystal X-ray diffraction measurements were conducted using a Rigaku Mercury CCD diffractometer with graphite monochromated Mo Kα radiation (λ = 0.71069 Å) and a rotating anode generator. Each single crystal was mounted on a MicroMount using paraffin oil. The crystal was then cooled using a N_2-flow-type temperature controller. Diffraction data were collected and processed using the CrystalClear software.[42] Structures were solved by the direct method using SIR-2004 for **Cu_2I_2-[O,O]** and SIR-92 for **Cu_2Br_2-[O,O]**.[43,44] Structural refinements were conducted by the full-matrix least-squares method using SHELXL-97.[45] Non-hydrogen atoms were refined anisotropically, hydrogen atoms were refined using the riding model. All calculations were conducted using the Crystal Structure crystallographic software package.[46] Crystallographic data obtained for each complex are summarized in Table 1.

Table 1. Crystal Parameters and Refinement Data

complex	**Cu_2I_2-[O,O]**	**Cu_2Br_2-[O,O]**
T/K	150(1)	150(1)
formula	$C_{40}H_{42}Cu_2I_2O_2P_2S_2$	$C_{40}H_{42}Cu_2Br_2O_2P_2S_2$
formula weight	1061.74	967.74
crystal system	triclinic	triclinic
space group	$P\bar{1}$	$P\bar{1}$
a/Å	8.627(3)	8.5094(9)
b/Å	9.354(3)	9.1692(11)
c/Å	14.551(4)	14.637(2)
α/deg	91.046(3)	89.327(7)
β/deg	103.948(3)	75.285(6)
γ/deg	116.074(3)	63.713(5)
V/Å^3	1013.2(5)	983.6(3)
Z	1	1
D_{cal}/ g cm^{-3}	1.740	1.634
reflns collected	8240	7991
unique reflns	4553	4432
R_{int}	0.0170	0.0168
GOF	1.072	1.056
R ($I > 2.00\sigma(I)$)	0.0270	0.0253
R_W[a]	0.0651	0.0656

[a] $R_W = [\sum(w(F_o^2 - F_c^2)^2)/\sum w(F_o^2)^2]^{1/2}$.

Luminescence Properties. The luminescence spectrum of each sample was acquired at room temperature using a JASCO FR-6600 spectrofluorometer. The excitation and emission slit widths were set to 5 and 6 nm, respectively. The luminescence quantum efficiency was recorded on a HAMAMATSU C9920-02 absolute photoluminescence quantum yield measurement system equipped with an integrating sphere apparatus and a 150 W CW xenon light source. The emission lifetime and time-resolved spectra were assessed using a streak camera (Hamamatsu Photonics, C4334) as a photodetector under 355 nm excitation (LOTIS TII Ltd., 355 nm). A liquid N_2 cryostat (Optistat-DN optical Dewar and ITC-503 temperature controller, Oxford Instruments) was used to control the sample temperature.

UV−vis Spectroscopy. The UV−vis absorption spectrum of each complex was recorded on a Shimadzu UV-2500PC or a Multispec-1500 spectrophotometer. The diffuse reflectance spectrum of each complex was recorded on the Shimadzu UV-2500PC spectrophotometer equipped with an integrating sphere apparatus. The obtained reflectance spectra were converted to absorption spectra using the Kubelka−Munk function $F(R_\infty)$.

Thermogravimetric Analysis. Thermogravimetry and differential thermal analysis were conducted using a Rigaku ThermoEvo TG8120 analyzer.

IR Spectroscopy. For IR absorption measurements, samples were prepared by grinding the powdered samples with KBr, after which, the samples were analyzed using a JASCO FT-IR 4100 spectrophotometer. Temperature-dependent IR spectra were acquired using a Nicolet 6700 FT-IR spectrometer with a Nicolet Continuum microscope. The sample temperature was controlled by a Linkam LK-600 hot stage.

Powder X-ray Diffraction. Powder X-ray diffraction was conducted using a Rigaku SmartLab diffractometer with Cu Kα radiation (λ =1.5405 Å) and a D/teX one-dimensional SSD detector. The sample temperature was controlled using a low-temperature

chamber (Anton Paar, TTK-450) coupled with a temperature control unit (Anton Paar, TCU-110).

Theoretical Calculations. Density functional theory (DFT) calculations were performed on a 2CPU workstation UNIV-D2G/Silent. Geometry optimization was achieved using the Becke3LYP functional[47,48] and LANL2DZ basis set[49−52] for all complexes studied in this work with a restricted Hartree−Fock formalism. All DFT calculations were performed using the Gaussian 03 program (Revision E.01-SMP).[53]

Photoirradiation Experiments. Photoirradiation experiments were conducted using a Perfect UV LAX-103 light source (Asahi Spectra Inc.) with optical filters (band-pass-type filters XBPA-300, XBPA-400, and XBPA-500).

RESULTS AND DISCUSSION

Crystal Structures. Figure 1 shows the molecular structure of $\mathbf{Cu_2I_2}$-[O,O] at 150 K. Selected bond lengths and angles are

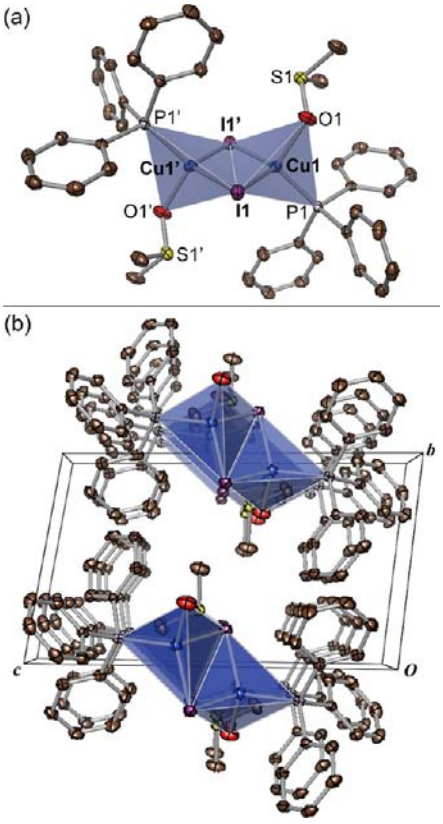

Figure 1. (a) Molecular structure of $\mathbf{Cu_2I_2}$-[O,O] and (b) packing diagram viewed along the *a* axis with thermal vibrational ellipsoids at 50% probability at 150 K. The coordination spheres of the Cu(I) ions are shown as blue tetrahedrons. Hydrogen atoms are omitted for clarity.

shown in Table 2. The $\mathbf{Cu_2I_2}$-[O,O] and $\mathbf{Cu_2Br_2}$-[O,O] complexes are isomorphous and crystallized in the triclinic $P\bar{1}$ space group. These complexes are characterized by a $\{Cu_2(\mu\text{-}X)_2\}$ (X = I^-, Br^-) rhombus as a structural unit, with one PPh_3 and one DMSO ligand coordinated to each Cu ion. The $\{Cu_2(\mu\text{-}X)_2\}$ unit is planar with the crystallographic inversion center coinciding with the midpoint of the Cu−Cu vector. The Cu ion adopts a tetrahedral coordination geometry, comprising two halide ions, one P atom of PPh_3, and one O atom of DMSO, indicating that the oxidation state of Cu is monovalent. Notably, the DMSO unit, a well-known ambidentate ligand, is not bonded by the relatively soft S atom, but instead by the

Table 2. Selected Bond Lengths and Angles of $\mathbf{Cu_2I_2}$-[O,O] and $\mathbf{Cu_2Br_2}$-[O,O][a]

	$\mathbf{Cu_2I_2}$-[O,O]	$\mathbf{Cu_2Br_2}$-[O,O]
Cu1−X1	2.6174(8)	2.4674(5)
Cu1−X1′	2.6526(7)	2.5191(4)
Cu1−P1	2.230(1)	2.1990(7)
Cu1−O1	2.133(2)	2.125(1)
Cu1−Cu1′	2.9980(6)	3.1111(5)
X1−X1′	4.3343(9)	3.8974(5)
Cu1−X−Cu1′	69.340(16)	77.194(14)
X1−Cu1−X1′	110.660(15)	102.806(13)

[a]Symmetry operation ′: −*x*, −*y*, −*z*.

relatively hard O atom. The Cu−X and Cu−P bond distances in both $\mathbf{Cu_2X_2}$-[O,O] complexes are close to those observed in the tetranuclear *cubane*-type clusters $[Cu_4(\mu_3\text{-}X)_4(PPh_3)_4]$ (*c*-$\mathbf{Cu_4X_4}$: X = Br^- and I^-).[17,21] The bond distances between Cu(I) and the O atom of the DMSO ligand are independent of the halide ion. The notable differences between the two $\mathbf{Cu_2X_2}$-[O,O] complexes are the Cu−X−Cu bond angles and Cu···Cu distance in the rhombic unit; the Cu···Cu distance in the rhombic $\{Cu_2(\mu\text{-}X)_2\}$ unit is well-known to exert a significant impact on the photophysical properties of Cu(I)−halide cluster complexes. A short Cu···Cu distance of less than ca. 2.7 Å in cubane-type $\{Cu_4(\mu_3\text{-}X)_4\}$ clusters usually generates the emissive ^{3}CC (cluster-centered) state.[19,22] Although the Cu···Cu distance in $\mathbf{Cu_2I_2}$-[O,O] (2.9980(6) Å) is markedly shorter (by ca. 0.113 Å) than that in $\mathbf{Cu_2Br_2}$-[O,O] (3.1111(5) Å) probably due to the larger ionic radius of iodide relative to bromide, both distances are longer than that of the complexes with Cu···Cu distances shorter than twice the van der Waals radius of Cu (2.80 Å) that exhibit ^{3}CC emission. Notably, there are one-dimensional DMSO channels along the *a* axis, as shown in Figure 1b.

Thermal Structural Transformations. As the DMSO ligand is a weak and easily removable ligand, the thermal stability of the $\mathbf{Cu_2X_2}$-[O,O] complexes is evaluated first. Figure 2 shows the TG-DTA curves of the $\mathbf{Cu_2I_2}$-[O,O] and

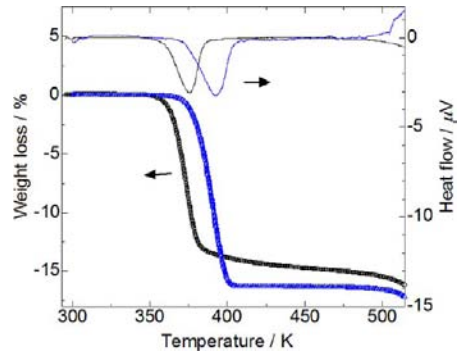

Figure 2. TG-DTA curves of (black lines) $\mathbf{Cu_2I_2}$-[O,O] and (blue lines) $\mathbf{Cu_2Br_2}$-[O,O] (1 K min^{-1} heating; Ar flow rate: 300 mL min^{-1}).

$\mathbf{Cu_2Br_2}$-[O,O] complexes in an Ar atmosphere. For both complexes, a steep and large weight loss is observed at ca. 373 K for $\mathbf{Cu_2I_2}$-[O,O] (13.6% loss) and 393 K for $\mathbf{Cu_2Br_2}$-[O,O] (16.0% loss). These weight losses are fairly consistent with the DMSO content of the complexes (14.7% for $\mathbf{Cu_2I_2}$-[O,O] and 16.2% for $\mathbf{Cu_2Br_2}$-[O,O]). An endothermic peak is also

dx.doi.org/10.1021/ic402104q | *Inorg. Chem.* 2013, 52, 13188−13198

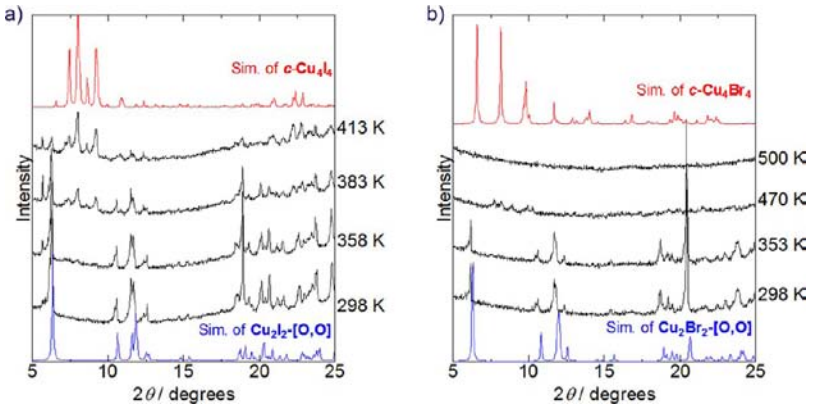

Figure 3. Temperature dependence of the PXRD patterns of (a) Cu_2I_2-[O,O] and (b) Cu_2Br_2-[O,O] complexes. The blue line at the bottom and red line at the top show the simulation patterns of Cu_2X_2-[O,O] and cubane-type cluster complexes *c*-Cu_4X_4 (X = I^-, Br^-),[17,21] respectively.

observed at the weight-loss temperature for both complexes. The IR bands assigned to the DMSO ligand completely disappear when the samples are heated at these temperatures (see Figure S1, Supporting Information), confirming that all coordinating DMSO ligands can be completely removed within these temperature regions. Based on the fact that these weight-loss temperatures are remarkably lower than the boiling point of DMSO (462 K), the coordination between the Cu(I) ion and DMSO is thought to be weak. The slightly higher removal temperature of Cu_2Br_2-[O,O] relative to Cu_2I_2-[O,O] is plausibly due to the tighter packing in the former; that is, the volume occupied by the DMSO ligand in one unit cell of the Cu_2Br_2-[O,O] crystal (188.6 $Å^3$ calculated using Platon SQUEEZE)[54] is smaller than that in the Cu_2I_2-[O,O] crystal (206.9 $Å^3$). These complexes gradually decompose above 500 K. Powder X-ray diffraction (PXRD) measurements are used to investigate the structures after DMSO removal. Figure 3 shows the temperature dependences of the PXRD patterns of the Cu_2I_2-[O,O] and Cu_2Br_2-[O,O] complexes. Before removal of DMSO, the diffraction patterns of both complexes are almost identical to the simulated patterns based on their crystal structures. The PXRD patterns gradually change above DMSO-removal temperatures. Interestingly, the PXRD patterns of Cu_2I_2-[O,O] at temperatures higher than the DMSO removal temperature are consistent with the simulated pattern based on the single crystal data[21] for the cubane-type cluster, *c*-Cu_4I_4, indicating the formation of *c*-Cu_4I_4 upon thermal removal of the DMSO ligand. In contrast, the PXRD pattern of Cu_2Br_2-[O,O] at 470 K, which is above the DMSO removal temperature (>410 K), is a featureless, amorphous pattern that is not consistent with the simulated pattern for the corresponding cubane-type Cu(I) cluster complex, *c*-Cu_4Br_4.[17] The reason why Cu_2I_2-[O,O] can be converted to the cubane-type cluster *c*-Cu_4I_4 but Cu_2Br_2-[O,O] cannot be converted to the corresponding one may be attributed to the structural dissimilarity between Cu_2X_2-[O,O] and *c*-Cu_4X_4. For example, the Cu−I−Cu bond angle in Cu_2I_2-[O,O] (69.34(2)°) falls within the range of the bond angles of *c*-Cu_4I_4 (65.3−70.5°),[21] whereas the bond angle in Cu_2Br_2-[O,O] (77.19(2)°) is significantly smaller than that in *c*-Cu_4Br_4 (83.5−90.2°).[17] This large structural difference between Cu_2Br_2-[O,O] and *c*-Cu_4Br_4 implies that the activation energy for structural transformation from the DMSO-released $Cu_2Br_2(PPh_3)_2$ to *c*-Cu_4Br_4 is higher than that for the iodide complex.

As mentioned in the Introduction, cubane-type Cu(I) cluster complexes are well-known to exhibit bright phosphorescence from the triplet cluster-centered (^{3}CC) excited state.[19,22] Certain Cu(I) cluster complexes with phosphine ligands exhibit interesting thermochromic luminescence, which is thought to originate from switching of the emissive excited state from the triplet mixed halide-to-ligand and metal-to-ligand charge transfer (mixed ^{3}XLCT and ^{3}MLCT) state to the ^{3}CC state.[21,22] Because Cu_2I_2-[O,O] forms the cubane-type cluster *c*-Cu_4I_4 after removal of DMSO, we investigated the photophysical properties of Cu_2X_2-[O,O]. Figure 4 shows the

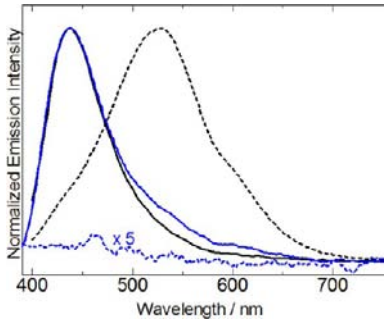

Figure 4. Luminescence spectra of Cu_2I_2-[O,O] (black lines) and Cu_2Br_2-[O,O] (blue lines) at room temperature. Solid and broken lines show the spectra before and after DMSO removal by heating at 423 K for 1 h, respectively. λ_{ex} = 350 nm.

luminescence spectra of Cu_2I_2-[O,O] and Cu_2Br_2-[O,O] before and after removal of DMSO by heating at 423 K for 1 day. Prior to DMSO removal, both complexes exhibit bright blue luminescence (Φ_{em} = 0.19 and 0.14, respectively) centered at 440 nm. The luminescence energy and very long luminescence lifetimes of these complexes (160 and 220 μs at 77 K, respectively) suggest that the blue luminescence plausibly originates from phosphorescence from the mixed ^{3}XLCT and ^{3}MLCT excited state. After thermal removal of DMSO, the blue emission of Cu_2I_2-[O,O] changes to a bright yellowish-green luminescence with a quite high luminescence quantum yield (Φ_{em} = 0.95). In addition, the temperature dependence of the luminescence spectrum of Cu_2I_2-[O,O] clearly shows a sudden change in the emission maximum within the DMSO-removal temperature range of 435−530 nm (see Figure S2, Supporting Information). These results are consistent with the thermal conversion of Cu_2I_2-[O,O] to *c*-

dx.doi.org/10.1021/ic402104q | Inorg. Chem. 2013, 52, 13188−13198

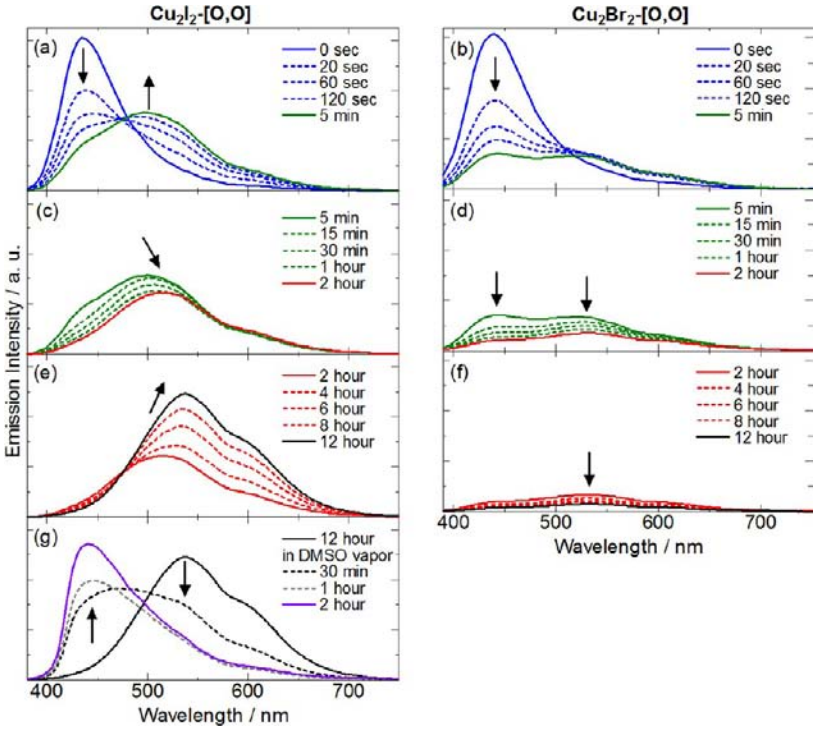

Figure 5. Luminescence spectral changes of (left) Cu_2I_2-[O,O] and (right) Cu_2Br_2-[O,O] crystals under UV light irradiation at room temperature. (a, b) UV light irradiation time from 0 to 5 min, (c, d) 5 min to 2 h, (e, f) 2 to 12 h, and (g) in the presence of saturated DMSO vapor without UV light irradiation. Wavelengths of both irradiation and excitation light are 350 nm. Scan speed of emission wavelength is 20 000 nm/min.

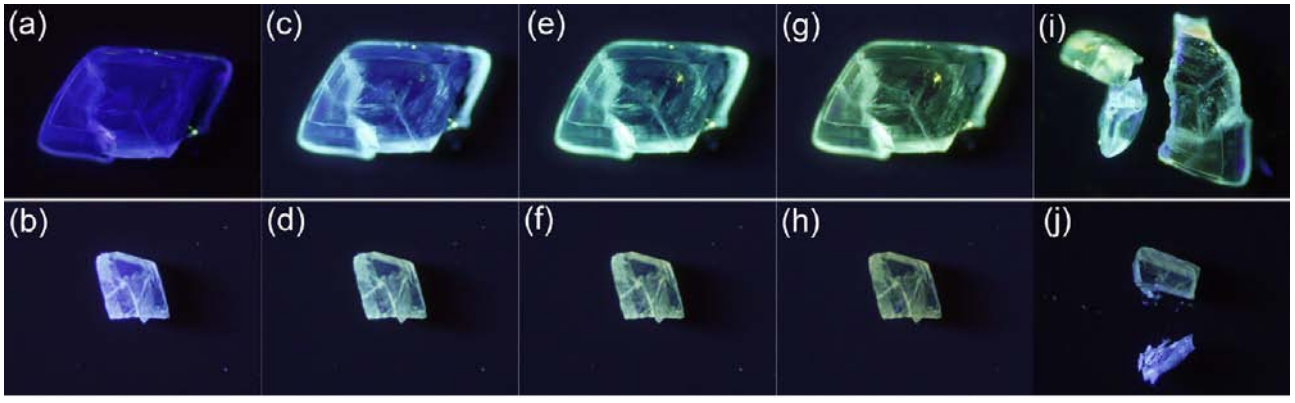

Figure 6. Images showing the change in the luminescence in Cu_2I_2-[O,O] (upper: a, c, e, g, i) and Cu_2Br_2-[O,O] (lower: b, d, f, h, j) crystals at 298 K: (a, b) before UV light irradiation (0 min; λ_{irr} = 300 nm), (c, d) after irradiation for 10 min, (e, f) 30 min, (g, h) 2 h, and (i, j) cleavage planes of the UV-irradiated (2 h) crystals, respectively.

Cu_4I_4, which shows yellow-green emission from the ^{3}CC excited state.[22] In contrast, in the case of Cu_2Br_2-[O,O], the initial blue emission almost disappears upon removal of DMSO as a result of formation of the amorphous form, with no further change.

Photochromic Luminescence. As previously stated, DMSO may function as an ambidentate ligand,[36−38] and thus at least two possible linkage isomers (S-bonded and O-bonded) are possible for DMSO-coordinated metal complexes. Certain Ru(II) complexes containing the DMSO ligand exhibit photoinduced linkage isomerization in the solution state.[36,37] Due to the presence of the DMSO ligand in the Cu(I) complexes, Cu_2I_2-[O,O] and Cu_2Br_2-[O,O], we evaluated the possibility of the photoinduced linkage isomerization among three possible isomers, Cu_2X_2-[O,O], Cu_2X_2-[O,S], and Cu_2X_2-[S,S]. Figure 5 shows the luminescence spectral changes for Cu_2I_2-[O,O] and Cu_2Br_2-[O,O] crystals under UV irradiation at 298 K. Changes in the luminescence of the Cu_2I_2-[O,O] crystal are shown in Figure 6. Interestingly, the luminescence spectra of both complexes change dramatically under UV irradiation. Within the first 5 min of irradiation (1st step), the intensity of the initial blue emission bands of both complexes centered at 435 nm decreases very rapidly, as shown in Figure 5a,b. A new, broad, green emission band appears at ca. 500 nm for Cu_2I_2-[O,O], whereas such an emission is not observed for Cu_2Br_2-[O,O]. In the irradiation period between 5 min and 2 h (2nd step), the newly developed green emission band of Cu_2I_2-[O,O] gradually shifts by about 14 nm to lower energy (Figure 5c). In contrast, the emission of Cu_2Br_2-[O,O] is simply weakened by UV irradiation (Figure 5d). Upon further UV irradiation for more than 2 h (3rd step), the emission band of Cu_2I_2-[O,O] slowly shifts to lower energy (by

dx.doi.org/10.1021/ic402104q | Inorg. Chem. 2013, 52, 13188−13198

about 23 nm) and the intensity increases remarkably (Figure 5e), whereas the emission of Cu_2Br_2-[O,O] almost disappears (Figure 5f). It is noteworthy that the initial blue emission of Cu_2I_2-[O,O] at 435 nm can be recovered by exposure to saturated DMSO vapor for several hours at 298 K without UV light irradiation (Figure 5g). These intriguing results clearly demonstrate that the luminescence properties of the iodide-bridged complex Cu_2I_2-[O,O] can be manipulated by light irradiation and exposure to DMSO vapor, whereas the luminescence of the isomorphous complex Cu_2Br_2-[O,O] simply disappears probably due to photothermal damage.[55] The remarkable difference between the emission properties of Cu_2I_2-[O,O] and Cu_2Br_2-[O,O] after prolonged irradiation indicates that the bridging halide ion plays an important role in determining the emission properties of these complexes. In addition, the recovery of the initial blue emission of Cu_2I_2-[O,O] in the presence of saturated DMSO vapor implies that the photochromic behavior is deeply related to certain motions or rearrangements of the ambidentate DMSO ligand. It should be noted that the UV−vis diffuse reflectance spectrum and powder X-ray diffraction pattern of Cu_2I_2-[O,O] are almost intact after prolonged UV irradiation (see Figures S3 and S4, Supporting Information), implying that the photoinduced structural transformations do involve the bulk crystals but occur only near the crystal surfaces. In fact, the emission color of the Cu_2I_2-[O,O] and Cu_2Br_2-[O,O] crystals changes from blue to yellowish-green upon UV irradiation, as shown in Figure 6a−h, but the color of the emission from within the crystal is still blue after prolonged irradiation (see Figure 6i,j). This provides direct evidence that the photoinduced structural transformation occurs only at the crystal surface.

To investigate the photochromic behavior of Cu_2I_2-[O,O] in more detail, the relationship between the UV (λ = 350 nm) irradiation time and the emission maxima (λ_{em}) of the Cu_2I_2-[O,O] crystals at several temperatures was investigated. As shown in Figure 7, the initial blue emission at ca. 435 nm

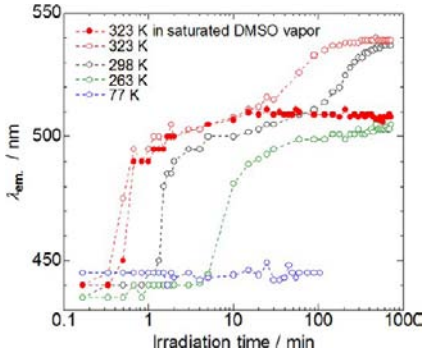

Figure 7. Relationship between UV light (λ = 350 nm) irradiation time and the emission maxima (λ_{em}) of Cu_2I_2-[O,O] crystals at 77 K in air (blue open circles), 263 K in air (green open circles), 298 K in air (black open circles), 323 K in air (red open circles), and 323 K with the presence of saturated DMSO vapor (red closed circles).

remains unchanged upon UV irradiation at 77 K. Above 263 K, the rapid emission changes corresponding to the first and second steps are observed within 10 min of irradiation. At 323 and 298 K, the emission maximum of Cu_2I_2-[O,O] gradually shifts to about 540 nm. On the other hand, this third step change is completely suppressed by lowering the temperature to 263 K or in the presence of saturated DMSO vapor. It should be noted that the emission spectral changes occur faster at higher temperatures than those at lower temperature, suggesting that these photochromic behaviors are assisted by some thermal excitation processes in the photoexcited state. Figure 8a shows the emission decay curves of the Cu_2I_2-[O,O] crystals at 77 K before and after UV irradiation for 3 h. Initially, the emission lifetime of the Cu_2I_2-[O,O] is relatively long at ca. 160 μs, whereas a shorter-lived component (2−30 μs) is apparent after UV irradiation for 3 h (note that the lifetime measurements are conducted at 77 K to suppress the photoreaction during the measurement, but the UV irradiation is performed at 298 K). Notably, the steady-state emission maximum of the UV-irradiated Cu_2I_2-[O,O] crystals change from 540 to 450 nm when the temperature is lowered to 77 K. The time-resolved emission spectra of this UV-irradiated Cu_2I_2-[O,O] (Figure 8b) clearly reveal the coexistence of two different emissive species with emission maxima at 470 and 540 nm at this temperature. The emission maximum of the spectrum acquired before 72 μs decay is observed at 522 nm, whereas the emission maximum is observed at 470 nm at longer times (72−500 μs). This longer-lived, high-energy emission species completely disappears when the temperature is increased to 298 K, suggesting that there is an activation barrier between these two emission states. Considering the fact that the ^{3}CC emission of the *c*-Cu_4I_4 cluster (λ_{em} = 545 nm, τ_{em} = 4.3 μs at 290 K)[22] is very similar to that of the long-time UV-irradiated Cu_2I_2-[O,O] crystals (λ_{em} = 540 nm, τ_{em} ~ 1 μs at 298 K), the origin of the emission of the Cu_2I_2-[O,O] species changes from the mixed ^{3}XLCT and ^{3}MLCT to the ^{3}CC excited state upon UV irradiation.

The structural transformation induced by UV irradiation is investigated by monitoring the IR spectral change of Cu_2I_2-[O,O] under UV irradiation at 298 K (Figure 9). Compared with the spectra of the *c*-Cu_4I_4 generated after thermal removal of DMSO, the strong absorption peaks in the spectrum of Cu_2I_2-[O,O] at 1002 and 946 cm^{-1} can be easily assigned to the DMSO ligand. The ν(S═O) vibration of the DMSO ligand depends on its coordination mode; that is, the frequency of the ν(S═O) mode is commonly shifted to lower frequency for O-coordinated DMSO relative to the bulk liquid.[56] The ν(S═O) frequency of the Cu_2I_2-[O,O] complex (1002 cm^{-1}) is lower than that of bulk DMSO (1050 cm^{-1}), consistent with the O-coordinated X-ray structures of these complexes. Interestingly, UV irradiation induces the gradual appearance of three new absorption peaks (at 1120, 721, and 540 cm^{-1}), which are ascribed to the photoinduced structural transformation. These peaks are also observed at almost the same frequency for Cu_2I_2-[O,O] containing deuterated DMSO, prepared from d_6-DMSO solvent (see Figure S5, Supporting Information), suggesting that the bands are not related to the C−H bond vibrations. Thus, the most plausible transformation is linkage isomerization of the DMSO ligand from the O-coordinated mode to the S-coordinated mode to form the S-coordinated isomers Cu_2I_2-[O,S] and/or Cu_2I_2-[S,S]. In fact, the observed frequency (1120 cm^{-1}) is highly consistent with the ν(S═O) frequency region of the S-coordinated DMSO ligands.[57,58] The two other peaks (720 and 540 cm^{-1}) are tentatively assigned to the ring vibrations of the PPh_3 ligands, which are affected by the linkage isomerization of the DMSO ligand. It should be noted that the IR spectral changes under UV light irradiation occurred considerably slower than those observed with emission spectroscopy. Given that the PXRD patterns and UV−vis diffuse reflectance spectrum of Cu_2I_2-[O,O] show little variation upon UV irradiation for 1 day or more (see Figures

dx.doi.org/10.1021/ic402104q | Inorg. Chem. 2013, 52, 13188−13198

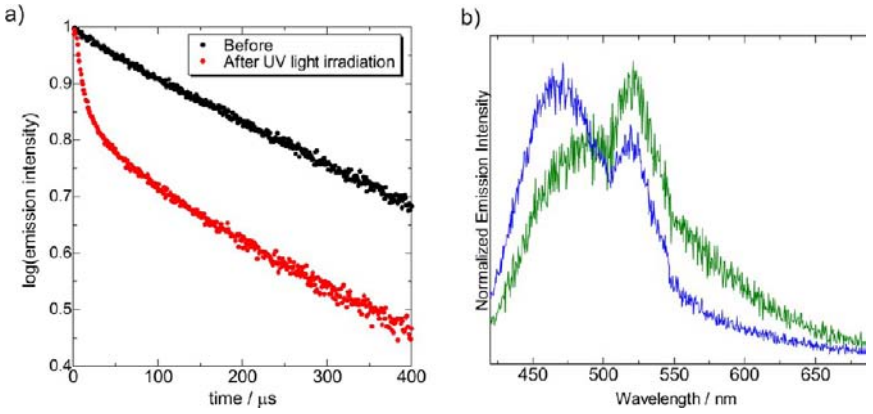

Figure 8. (a) Emission decays of Cu_2I_2-[**O,O**] crystals at 77 K (λ_{ex} = 335 nm): before (black) and after (red) the UV light irradiation for 3 h (λ_{irr} = 350 nm). (b) Time-resolved emission spectra at 77 K for the UV-light-irradiated Cu_2I_2-[**O,O**] for 3 h. Green and blue spectra were taken before and after 72 μs decay, respectively.

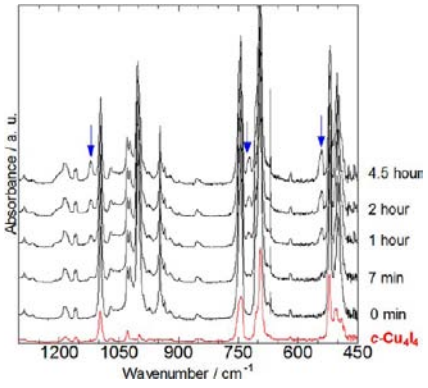

Figure 9. IR spectral changes of Cu_2I_2-[**O,O**] under UV light irradiation at 298 K (λ_{irr} = 300 nm). The bottom red line shows the IR spectrum of the thermally DMSO-removed sample prepared by heating Cu_2I_2-[**O,O**] for 1 day in an Ar atmosphere. Blue arrows indicate newly appeared peaks on UV irradiation.

S3 and S4, Supporting Information), the photoinduced structural transformation involving linkage isomerization of the DMSO ligand occurs only near the crystal surface. Emission spectroscopy is very sensitive to microscopic modifications, such as surface defects and impurities in a crystalline material. Thus, the time required to detect structural changes using emission spectroscopy is much less than that required for IR spectroscopy, which considers the entirety of the crystalline material.

Theoretical Calculations. As discussed above, the iodide-bridged rhombic dicopper(I) complex, Cu_2I_2-[**O,O**], shows a bright blue emission and drastic luminescence changes upon UV irradiation. The IR spectral changes induced by UV irradiation suggest that UV irradiation induces linkage isomerization from the O-coordinated Cu_2X_2-[**O,O**] to S-coordinated Cu_2X_2-[**S,S**] (and/or Cu_2X_2-[**S,O**]) species. Upon prolonged UV irradiation, the DMSO ligand is photothermally released. This photochromic behavior is evaluated based on DFT

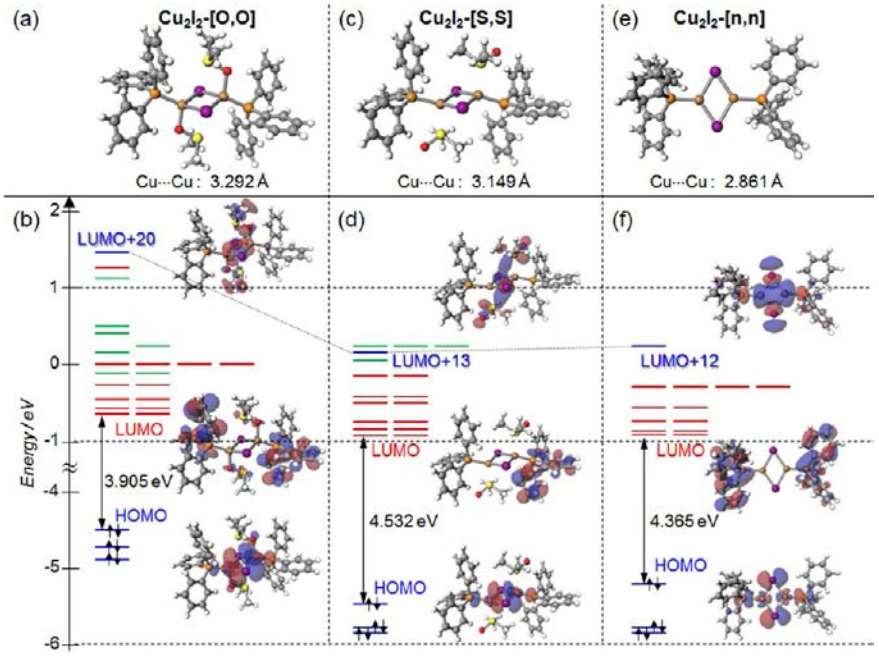

Figure 10. Geometry-optimized molecular structures and schematic MO diagrams of (a, b) Cu_2I_2-[**O,O**], (c, d) Cu_2I_2-[**S,S**], and (e, f) DMSO-removed Cu_2I_2-[**n,n**]. Each energy level in (b, d, f) was colored according to the main components: blue, $Cu_2(\mu\text{-}I)_2$ core; red, PPh_3; green, DMSO.

dx.doi.org/10.1021/ic402104q | *Inorg. Chem.* 2013, 52, 13188−13198

calculations for the following three forms: the O-coordinated **Cu_2I_2-[O,O]** as the initial state; the linkage isomer **Cu_2I_2-[S,S]** with two S-coordinated DMSO ligands; and the DMSO-removed dinuclear complex $[Cu_2(\mu\text{-}I)_2(PPh_3)_2]$ (abbreviated as **Cu_2I_2-[n,n]**). The changes in the IR spectra of **Cu_2I_2-[O,O]** under UV irradiation suggest that the latter two forms are possible candidates as the green and/or yellowish-green emitting species. The geometry is optimized using the Becke3LYP functional[47,48] and LANL2DZ basis sets[49−52] for all three structures. The structural parameters obtained from the DFT calculation are summarized in Table S1 (Supporting Information). Cartesian coordinates of the three models, **Cu_2I_2-[O,O]**, **Cu_2I_2-[S,S]**, and **Cu_2I_2-[n,n]**, are listed in Tables S2, S3, and S4 (Supporting Information). Figure 10 shows the optimized molecular structures and schematic MO diagrams of the near frontier orbitals of the three models. The calculated bond distances and angles of the initial **Cu_2I_2-[O,O]** are in fair agreement with the X-ray structure of **Cu_2I_2-[O,O]** considering the general slight overestimation of the computed distances and angles (see Table S1 in the Supporting Information). As shown in Figure 10b, the highest occupied molecular orbital (HOMO) of **Cu_2I_2-[O,O]** mainly comprises the copper and iodide orbitals of the central $Cu_2(\mu\text{-}I)_2$ core with the lone pair electrons of the P atom of the PPh_3 ligand, whereas the lowest unoccupied molecular orbital (LUMO) comprises almost pure PPh_3 π^* orbitals. The LUMO+1 to LUMO+7 orbitals are also localized on the PPh_3 ligand. MOs derived primarily from the DMSO ligand are located on and above the upper edge of this block of PPh_3-based MOs (LUMOs + 8, +9, +14 ∼ +17). The Cu···Cu bonding orbital with some Cu−I antibonding character is found as LUMO+20 above these PPh_3- and DMSO-based MOs. As expected from the molecular structure of **Cu_2I_2-[O,O]**, the long Cu···Cu distance (2.9980(6) Å in the X-ray structure) compared to twice the van der Waals radius of Cu (2.80 Å) weakens the Cu···Cu interaction, leaving this bonding orbital at higher energy.

Cu_2I_2-[S,S] is quite different from **Cu_2I_2-[O,O]**, as shown in Figure 10c. The distances between the Cu(I) ion and the S atom of the DMSO ligand (2.7077 and 2.6976 Å) are longer than those found in a Cu(I) coordination polymer containing the S-coordinated DMSO ligand $[Cu_2Cl_2\{^tBuNP(o\text{-}OC_6H_4\text{-}OMe)\}_2(DMSO)_2]_n$,[59] suggesting that the two DMSO ligands do not form coordination bonds. Nevertheless, these distances are shorter than the sum of the van der Waals radii of the Cu and S atoms (3.25 Å), indicating that the DMSO ligands may be trapped near the Cu(I) ion by van der Waals contact. The change in the coordination mode of the DMSO ligand exerts a considerable effect on other structural parameters. For instance, the calculated Cu−I bond distances (*mean* 2.736 Å) are ca. 0.09 Å shorter than those of **Cu_2I_2-[O,O]**. Notably, the Cu···Cu distance of the rhombic $\{Cu_2(\mu\text{-}I)_2\}$ unit (3.149 Å) is markedly shorter (by about 0.144 Å) than the calculated value for **Cu_2I_2-[O,O]**. Because of this significant structural transformation, the electronic structure of **Cu_2I_2-[S,S]** as shown in Figure 10d is also different from that of **Cu_2I_2-[O,O]**. Although the HOMO and LUMO are mainly localized on the $\{Cu_2(\mu\text{-}I)_2\}$ core and the PPh_3 ligand in **Cu_2I_2-[S,S]** as is the case for **Cu_2I_2-[O,O]**, shrinkage of the $\{Cu_2(\mu\text{-}I)_2\}$ core stabilizes the HOMOs by about 0.9 eV compared to that of **Cu_2I_2-[O,O]**. The π^* orbitals of the PPh_3 ligand near the LUMO are also stabilized by about 0.3 eV, resulting in a larger HOMO−LUMO gap for the S-coordinated form (by about 0.6 eV) relative to **Cu_2I_2-[O,O]**. Interestingly, the bonding orbital between the two Cu centers with some Cu−I antibonding character is found as LUMO+13 just above the upper edge of the π^*-orbital levels of the PPh_3 ligand. The energy gap between LUMO+13 and the LUMO (1.14 eV) is estimated to be significantly smaller (about 1.0 eV) than that of **Cu_2I_2-[O,O]** (2.13 eV) probably due to the shorter Cu−Cu distance. Notably, this energy separation is comparable to that of the DMSO-removed form, **Cu_2I_2-[n,n]**, having a considerably shorter Cu−Cu distance (2.861 Å; see below). As shown in Figure 10d, the shape of LUMO+13 implies that the bridging effect between the two Cu centers via the sulfur orbitals of the DMSO ligands may play an important role.

As shown in Figure 10e, the Cu ions adopt a trigonal-planar coordination geometry in the DMSO-removed form, **Cu_2I_2-[n,n]**. The calculated Cu−I bond distances are ca. 0.05 Å shorter than those in **Cu_2I_2-[S,S]**, whereas the Cu−P bond distances are comparable in both **Cu_2I_2-[O,O]** and **Cu_2I_2-[S,S]**. The Cu−Cu distance in the rhombic unit (2.861 Å) is also shortened relative to that in **Cu_2I_2-[S,S]** by about 0.2 Å. However, the electronic structure of the DMSO-removed form is similar to that of **Cu_2I_2-[S,S]**, except for the absence of the orbitals of the DMSO ligand, as shown in Figure 10f. As in the other two forms, the HOMO and the LUMO are localized on the rhombic $\{Cu_2(\mu\text{-}I)_2\}$ unit and the PPh_3 ligand, respectively. The HOMO−LUMO gap is ca. 0.17 eV higher than that in **Cu_2I_2-[S,S]**. The Cu−Cu bonding orbital is found to be LUMO+12, which is located above the upper edge of the π^* orbitals of the PPh_3 ligand. The energy separation between this Cu−Cu bonding orbital and the LUMO is estimated to be 1.20 eV, which is comparable to that in **Cu_2I_2-[S,S]**.

Possible Mechanism of Photochromic Luminescence. On the basis of the aforementioned discussion, the emission of **Cu_2I_2-[O,O]** changes dramatically in response not only to heating but also to UV light irradiation and exposure to DMSO vapor, as summarized in Scheme 1a. In this section, we discuss the possible mechanism of the photo- and vapor-controlled emission behaviors of **Cu_2I_2-[O,O]**.

Araki et al. reported the widely tunable luminescence of dinuclear copper(I) complexes, $Cu_2(\mu\text{-}X)_2(PPh_3)_2(L)_2$ (L = N-heteroaromatic ligand), from red to blue emission, originates from the mixed ^{3}XLCT and ^{3}MLCT transition state (from the rhombic $\{Cu_2(\mu\text{-}X)_2\}$ core to the π^* orbital of the N-heteroaromatic ligand L).[3] In the **Cu_2I_2-[O,O]** complex, the ambidentate DMSO ligand is positioned at the L-site, which is more difficult to reduce than that of N-heteroaromatic ligands like bipyridine. Thus, the energy of the XLCT and MLCT mixed transition from the $\{Cu_2(\mu\text{-}I)_2\}$ core to the π^* orbital of DMSO is expected to be higher than that from the $\{Cu_2(\mu\text{-}I)_2\}$ core to the π^* orbital of the PPh_3 ligand. In fact, the results of the present time-dependent DFT calculations for **Cu_2I_2-[O,O]** suggest that the HOMO−LUMO transition is mostly forbidden and that the lowest singlet excited transition is the HOMO−LUMO+1 transition, with slight mixing with the HOMO−LUMO+8 transition (see Table S5, Supporting Information). As discussed above, the HOMO, LUMO+1, and LUMO+8 are d + p orbitals of the $\{Cu_2(\mu\text{-}I)_2\}$ core, vacant π^* orbitals of PPh_3, and of the DMSO ligand, respectively. Thus, UV irradiation of **Cu_2I_2-[O,O]** initially generates the ^{1}XLCT and ^{1}MLCT mixed transition (from the $\{Cu_2(\mu\text{-}I)_2\}$ core mainly to the PPh_3 ligand) state. Given that the Cu···Cu distances in **Cu_2X_2-[O,O]** are remarkably longer than twice the van der Waals radius of Cu, the ^{3}CC excited state should be more unstable than the ^{3}XLCT and ^{3}MLCT mixed state, resulting in blue emission from the ^{3}XLCT and ^{3}MLCT mixed state. This

dx.doi.org/10.1021/ic402104q | *Inorg. Chem.* 2013, 52, 13188−13198

Scheme 1. (a) Possible Mechanism of Light-, Vapor-, and Heat-Induced Structural Transformation of Cu_2I_2-[O,O]. (b) Simplified Energy Level Diagram of the Three Possible Forms, Cu_2I_2-[O,O], Cu_2I_2-[S,S], and Cu_2I_2-[n,n][a]

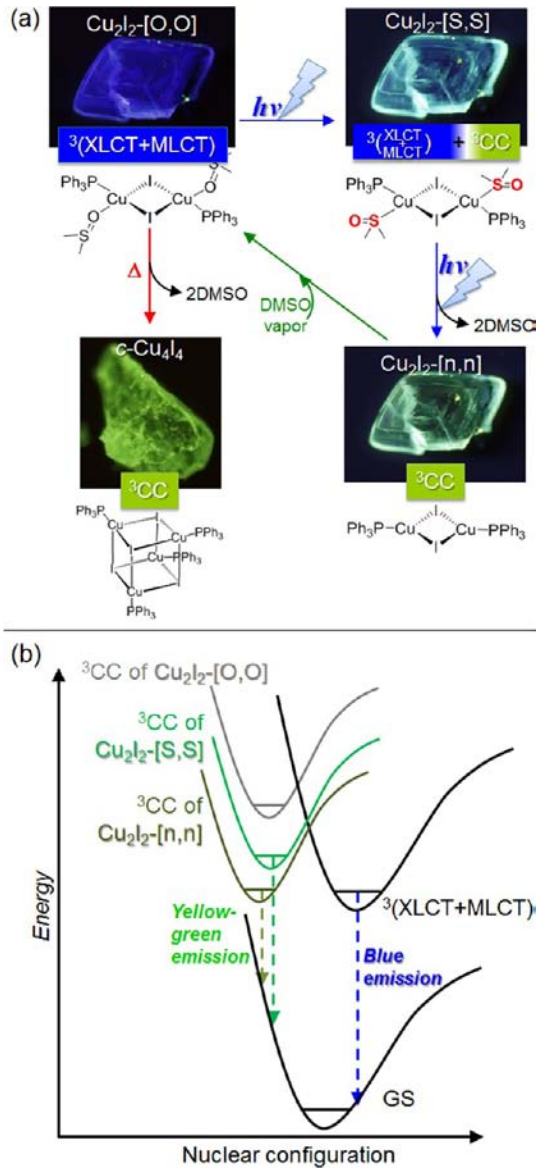

[a]To simplify the diagram, energy surfaces of the ground states and ^{3}XLCT and ^{3}MLCT mixed excited states of three forms are summarized in one curve, respectively.

blue emission from the ^{3}XLCT and ^{3}MLCT mixed state disappears quickly upon UV irradiation near room temperature, whereas this disappearance is completely suppressed by lowering the temperature to 77 K (Figure 7). In addition, IR spectroscopy suggests that linkage isomerization of DMSO from O-coordination to S-coordination occurs upon UV light irradiation (Figure 9). Thus, thermal excitation of the long-lived ^{3}XLCT and ^{3}MLCT mixed excited state should induce the linkage isomerization and/or removal of the DMSO ligand. The present DFT calculations for the linkage isomer **Cu_2X_2-[S,S]** and the DMSO-removed form **Cu_2X_2-[n,n]** suggest that these rearrangements of the DMSO ligand cause shrinkage of the $\{Cu_2(\mu\text{-}X)_2\}$ core to induce more effective Cu···Cu interaction (see Figure 10). In the shrunken **Cu_2I_2-[S,S]** and **Cu_2I_2-[n,n]** cores, the ^{3}CC state is more stable than that in the initial **Cu_2I_2-[O,O]** as shown in Scheme 1b. Consequently, the lower-energy yellowish-green emission from the ^{3}CC excited state gradually becomes allowed due to linkage isomerization and/or removal of the DMSO ligand. Given that the emission change in the third step is completely suppressed by lowering the temperature to 263 K or in the presence of saturated DMSO vapor, release of the DMSO ligand is the most plausible origin of this third step change. The first and second step changes are possibly due to photoinduced and thermally assisted linkage isomerization of the DMSO ligand from O-coordination to S-coordination (i.e., from **Cu_2I_2-[O,O]** to **Cu_2I_2-[S,S]** via **Cu_2I_2-[O,S]**). It should be noted that the ***c*-Cu_4I_4** complex obtained by heating **Cu_2I_2-[O,O]** at 423 K for 1 day is not converted to the original **Cu_2I_2-[O,O]** by exposure to DMSO vapor even at the relatively high temperature of 100 °C. Thus, the fact supports that the DMSO-removed form **Cu_2I_2-[n,n]** produced upon prolonged UV irradiation of the sample is not the cubane-type cluster ***c*-Cu_4I_4**, although the origin of the emission should be very similar to the ^{3}CC state of the cluster.

CONCLUSION

Two novel halide-bridged rhombic dicopper(I) complexes possessing the ambidentate DMSO ligand, $[Cu_2(\mu\text{-}X)_2(DMSO)_2(PPh_3)_2]$ (X = I^-, Br^-), were synthesized in this study. The luminescence of the iodide-bridged complex was sensitive to temperature as well as UV irradiation, and exposure to DMSO vapor. Simple reaction of CuX with PPh_3 in DMSO solution gave rise to colorless crystals of the O-coordinated linkage isomers, **Cu_2X_2-[O,O]**, which show bright blue phosphorescence (λ_{em} = 435 nm) from the ^{3}XLCT and ^{3}MLCT mixed excited state. Under UV irradiation, the blue phosphorescence of **Cu_2I_2-[O,O]** rapidly disappeared and a new green emission band simultaneously appeared at 500 nm. With prolonged irradiation, the emission color gradually changed to yellowish-green (λ_{em} = 540 nm); however, this change was completely suppressed by lowering the temperature to 263 K or in the presence of saturated DMSO vapor. Upon exposure of the UV-light-irradiated sample to DMSO vapor, the initial blue phosphorescence of **Cu_2I_2-[O,O]** was recovered. IR spectra acquired under UV irradiation suggest that linkage isomerization of the ambidentate DMSO ligand from the O-coordinated isomer, **Cu_2I_2-[O,O]**, to the S-coordinated isomers, **Cu_2I_2-[O,S]** and **Cu_2I_2-[S,S]**, occurs under UV irradiation, triggered by thermal excitation from the relatively long-lived ^{3}XLCT and ^{3}MLCT mixed state. Theoretical calculations suggest that both the linkage isomerization from O-coordination to S-coordination and the release of the DMSO ligand cause contraction of the rhombic $Cu_2(\mu\text{-}I)_2$ core, making the Cu···Cu interaction more effective. This contraction facilitates generation of the ^{3}CC emissive state by thermal excitation from the ^{3}XLCT and ^{3}MLCT mixed transition state, resulting in longer wavelength emission. The bromide-bridged complex, **Cu_2Br_2-[O,O]**, exhibits simple disappearance of blue phosphorescence from the ^{3}XLCT and ^{3}MLCT mixed state under UV irradiation, probably due to the longer Cu···Cu distance in the rhombic core than in **Cu_2I_2-[O,O]**. Further studies on concomitant bright emission and photochromic behavior based on emissive Cu(I) complexes are now in progress.

dx.doi.org/10.1021/ic402104q | *Inorg. Chem.* 2013, 52, 13188−13198

■ ASSOCIATED CONTENT

Supporting Information

X-ray crystallographic files of Cu_2I_2-[O,O] and Cu_2Br_2-[O,O] in CIF format; IR spectra of Cu_2Br_2-[O,O] before and after DMSO removal at 423 K; temperature dependence of the luminescence spectrum of Cu_2I_2-[O,O]; UV−vis diffuse reflectance spectra and powder X-ray diffraction pattern of Cu_2I_2-[O,O] before and after UV light irradiation; IR spectral change of Cu_2I_2-[O,O] bearing d_6-DMSO under UV light irradiation; selected bond lengths and angles of geometrically optimized Cu_2I_2-[O,O], Cu_2I_2-[S,S], and Cu_2I_2-[n,n]; and Cartesian coordinates of the optimized geometries for Cu_2I_2-[O,O], Cu_2I_2-[S,S], and Cu_2I_2-[n,n]; the result of TD-DFT calculation for Cu_2I_2-[O,O]. This material is available free of charge via the Internet at http://pubs.acs.org.

■ AUTHOR INFORMATION

Corresponding Author

*Tel: +81-11-706-3817. Fax: +81-11-706-3447. E-mail: mkato@sci.hokudai.ac.jp.

Notes

The authors declare no competing financial interest.

■ ACKNOWLEDGMENTS

The authors thank Dr. E. Sakuda and Prof. N. Kitamura (Hokkaido Univ.) for their valuable support of the emission lifetime measurements and time-resolved emission spectroscopy. This study was supported by a Grant-in-Aid for Scientific Research (B) (23350025), Photochromism (No. 471), Artificial Photosynthesis (No, 2406), Coordination Programming (No. 2107), Young Scientists (B) (24750049), and the Global COE Program (Project No. B01: Catalysis as the Basis for Innovation in Materials Science) from MEXT, Japan.

■ REFERENCES

(1) Ford, P. C.; Cariati, E.; Bourassa, J. *Chem. Rev.* **1999**, *99*, 3625−3647.
(2) Smith, C. S.; Branham, C. W.; Marquardt, B. J.; Mann, K. R. *J. Am. Chem. Soc.* **2010**, *132*, 14079−14085.
(3) Araki, H.; Tsuge, K.; Sasaki, Y.; Ishizaka, S.; Kitamura, N. *Inorg. Chem.* **2005**, *44*, 9667−9675.
(4) Hashimoto, M.; Igawa, S.; Yashima, M.; Kawata, I.; Hoshino, M.; Osawa, M. *J. Am. Chem. Soc.* **2011**, *133*, 10348−10351.
(5) Liu, Z.; Qayyum, M. F.; Wu, C.; Whited, M. T.; Djurovich, P. I.; Hodgson, K. O.; Hedman, B.; Solomon, E. I.; Thompson, M. E. *J. Am. Chem. Soc.* **2011**, *133*, 3700−3703.
(6) Igawa, S.; Hashimoto, M.; Kawata, I.; Yashima, M.; Hoshino, M.; Osawa, M. *J. Mater. Chem. C* **2013**, *1*, 542−551.
(7) McCormick, T.; Jia, W.-L.; Wang, S. *Inorg. Chem.* **2006**, *45*, 147−155.
(8) Cuttell, D. G.; Kuang, S.-M.; Fanwick, P. E.; McMillin, D. R.; Walton, R. A. *J. Am. Chem. Soc.* **2002**, *124*, 6−7.
(9) Omary, M. A.; Rawashdeh-Omary, M. A.; Diyabalanage, H. V. K.; Dias, H. V. R. *Inorg. Chem.* **2003**, *42*, 8612−8614.
(10) Czerwieniec, R.; Yu, J.; Yersin, H. *Inorg. Chem.* **2011**, *50*, 8293−8301.
(11) Smith, C. S.; Mann, K. R. *J. Am. Chem. Soc.* **2012**, *134*, 8786−8789.
(12) Araki, H.; Tsuge, K.; Sasaki, Y.; Ishizaka, S.; Kitamura, N. *Inorg. Chem.* **2007**, *46*, 10032−10034.
(13) Hirtenlehner, C.; Monokowius, U. *Inorg. Chem. Commun.* **2012**, *15*, 109−112.
(14) Sabin, F.; Ryu, C. K.; Ford, P. C.; Vogler, A. *Inorg. Chem.* **1992**, *31*, 1941−1945.
(15) Kyle, K. R.; Ryu, C. K.; DiBenedetto, J. A.; Ford, P. C. *J. Am. Chem. Soc.* **1991**, *113*, 2954−2965.
(16) Liu, Z.; Djurovich, P. I.; Whited, M. T.; Thompson, M. E. *Inorg. Chem.* **2012**, *51*, 230−236.
(17) Barron, P. F.; Dyason, J. C.; Engelhardt, L. M.; Healy, P. C.; White, A. H. *Inorg. Chem.* **1984**, *23*, 3766−3769.
(18) Vitale, M.; Ryu, C. K.; Palke, W. E.; Ford, P. C. *Inorg. Chem.* **1994**, *33*, 561−566.
(19) Angelis, F. D.; Fantacci, S.; Sgamellotti, A.; Cariati, E.; Ugo, R.; Ford, P. C. *Inorg. Chem.* **2006**, *45*, 10576−10584.
(20) Churchill, M. R.; Debore, B. G.; Donovan, D. J. *Inorg. Chem.* **1975**, *14*, 617−623.
(21) Kitagawa, H.; Ozawa, Y.; Toriumi, K. *Chem. Commun.* **2010**, *46*, 6302−6304.
(22) Perruchas, S.; Tard, C.; LeGoff, X. F.; Fargues, A.; Garcia, A.; Kahlal, S.; Saillard, J.-Y.; Gacoin, T.; Boilot, J.-P. *Inorg. Chem.* **2011**, *50*, 10682−10692.
(23) Hu, M.-C.; Wang, Y.; Zhai, Q.-G.; Li, S.-N.; Jiang, Y.-C.; Zhang, Y. *Inorg. Chem.* **2009**, *48*, 1449−1468.
(24) Wang, L.-Z.; Zhao, L.; Wang, D.-X.; Wang, M.-X. *J. Sold State Chem.* **2010**, *183*, 3010−3016.
(25) Braga, D.; Maini, L.; Mazzeo, P. P.; Venturam, B. *Chem.—Eur. J.* **2010**, *16*, 1553−1559.
(26) Bi, M.; Li, G.; Liu, Y.; Liu, X.; Hu, Y.; Shi, Z.; Feng, S. *Cryst. Growth Des.* **2007**, *7*, 2066−2070.
(27) Ren, S.-B.; Zhou, L.; Zhang, L.; Li, Y.-Z.; Du, H.-B.; You, X.-Z. *CrystEngComm* **2009**, *11*, 1934−1836.
(28) Hu, S.; Zhang, Z.-M.; Meng, Z.-S.; Lin, Z.-J.; Tong, M.-L. *CrystEngComm* **2010**, *12*, 4378−4385.
(29) Fomitchev, D. V.; Furlani, T. R.; Coppens, P. *Inorg. Chem.* **1998**, *37*, 1519−1526.
(30) Carducci, M. D.; Pressprich, M. R.; Coppens, P. *J. Am. Chem. Soc.* **1997**, *119*, 2669−2678.
(31) Kovalevsky, A. Y.; Bagley, K. A.; Coppens, P. *J. Am. Chem. Soc.* **2002**, *124*, 9241−9284.
(32) Basolo, F.; Burmeister, J. L.; Poe, A. J. *J. Am. Chem. Soc.* **1963**, *85*, 1700−1701.
(33) Jurisson, S.; Halihan, M. M.; Lydon, J. D.; Barnes, C. L.; Nowotnik, D. P.; Nunn, A. D. *Inorg. Chem.* **1998**, *37*, 1922−1928.
(34) Kishi, S.; Kato, M. *Inorg. Chem.* **2003**, *42*, 8728−8734.
(35) Kobayashi, A.; Fukuzawa, Y.; Chang, H.-C.; Kato, M. *Inorg. Chem.* **2012**, *51*, 7508−7519.
(36) Rack, J. J.; Mockus, N. V. *Inorg. Chem.* **2003**, *42*, 5792−5794.
(37) Rachford, A. A.; Petersen, J. L.; Rack, J. J. *Inorg. Chem.* **2005**, *44*, 8065−8075.
(38) Mockus, N. V.; Petersen, J. L.; Rack, J. J. *Inorg. Chem.* **2006**, *45*, 8−10.
(39) Nakai, H.; Mizuno, M.; Nishioka, T.; Koga, N.; Shiomi, K.; Miyano, Y.; Irie, M.; Breedlove, B. K.; Kinoshita, I.; Hayashi, Y.; Ozawa, Y.; Yonezawa, T.; Toriumi, K.; Isobe, K. *Angew. Chem., Int. Ed.* **2006**, *45*, 6473−6476.
(40) Sakamoto, R.; Murata, M.; Kume, S.; Sampei, H.; Sugimoto, M.; Nishihara, H. *Chem. Commun.* **2005**, 1215−1217.
(41) Anderson, C. P.; Salmon, D. J.; Meyer, T. J.; Young, R. C. *J. Am. Chem. Soc.* **1977**, *99*, 1980−1982.
(42) *CrystalClear*; Molecular Structure Corporation: Orem, UT, 2001.
(43) *SIR-2004*: Burla, M. C.; Caliandro, R.; Camalli, M.; Carrozzini, B.; Cascarano, G. L.; De Caro, L.; Giacovazzo, C.; Polidori, G.; Spagna, R. *J. Appl. Crystallogr.* **2005**, *38*, 381−388.
(44) *SIR-92*: Altomare, A.; Cascarano, G.; Giacovazzo, C.; Guagliardi, A.; Burla, M.; Polidori, G.; Camalli, M. *J. Appl. Crystallogr.* **1994**, *27*, 435−436.
(45) *SHELXL-97*: Sheldrick, G. M. *Acta Crystallogr., Sect. A: Found. Crystallogr.* **2008**, *64*, 112−122.
(46) *CrystalStructure 4.0: Crystal Structure Analysis Package*; Rigaku Corporation: Tokyo, Japan, 2000−2010.
(47) Becke, A. D. *J. Chem. Phys.* **1993**, *98*, 5648−5652.
(48) Lee, C.; Yang, W.; Parr, R. G. *Phys. Rev. B* **1993**, *37*, 785−789.

(49) Dunning, T. H., Jr.; Hay, P. J. In *Methods of Electronic Structure Theory*; Schaefer, H. F., III, Ed.; Modern Theoretical Chemistry; Plenum: New York, 1977; Vol. 3, pp 1−28.
(50) Hay, P. J.; Wadt, W. R. *J. Chem. Phys.* **1985**, *82*, 270−283.
(51) Wadt, W. R.; Hay, P. J. *J. Chem. Phys.* **1985**, *82*, 284−298.
(52) Hay, P. J.; Wadt, W. R. *J. Chem. Phys.* **1985**, *82*, 299−310.
(53) Frisch, M. J.; Trucks, G. W.; Schlegel, H. B.; Scuseria, G. E.; Robb, M. A.; Cheeseman, J. R.; Montgomery, J. A., Jr.; Vreven, J. T.; Kudin, K. N.; Burant, J. C.; Millam, J. M.; Iyengar, S. S.; Tomasi, J.; Barone, V.; Mennucci, B.; Cossi, M.; Scalmani, G.; Rega, N.; Petersson, G. A.; Nakatsuji, H.; Hada, M.; Ehara, M.; Toyota, K.; Fukuda, R.; Hasegawa, J.; Ishida, M.; Nakajima, T.; Honda, Y.; Kitao, O.; Nakai, H.; Klene, M.; Li, X.; Knox, J. E.; Hratchian, H. P. ; Cross, J. B.; Adamo, C.; Jaramillo, J.; Gomperts, R.; Stratmann, R. E.; Yazyev, O.; Austin, A. J.; Cammi, R.; Pomelli, C.; Ochterski, J. W.; Ayala, P. Y.; Morokuma, K.; Voth, G. A.; Salvador, P.; Dannenberg, J. J.; Zakrzewski, V. G. ; Dapprich, S.; Daniels, A. D.; Strain, M. C.; Farkas, O.; Malick, D. K.; Rabuck, A. D.; Raghavachari, K.; Foresman, F. B.; Ortiz, J. V.; Cui, Q.; Baboul, A. G.; Clifford, S.; Cioslowski, J.; Stefanov, B. B.; Liu, G.; Liashenko, A.; Piskorz, P.; Komaromi, I.; Martin, R. L.; Fox, D. J.; Keith, T.; Al-Laham, M. A.; Peng, C. Y.; Nanayakkara, A.; Challacombe, M.; Gill, P. M. W.; Johnson, B.; Chen, W.; Wong, M. W.; Gonzalez, C.; Pople, J. A. *Gaussian 03*, Revision E.01; Gaussian, Inc.: Wallingford, CT, 2004.
(54) Spek, A. L. *J. Appl. Crystallogr.* **2003**, *36*, 7−13.
(55) We examined the luminescence change of the UV-light irradiated **Cu_2Br_2**-[**O,O**] under DMSO vapor at several different temperatures, and found that the blue emission appeared again, but the response was much slower than that of **Cu_2I_2**-[**O,O**] and an additional emission band at 530 nm was also observed (see Figure S6 shown in the Supporting Information). Thus, the re-adsorption of DMSO vapor can occur to form the original blue emissive **Cu_2I_2**-[**O,O**], whereas the different chemical reaction might occur in parallel with the re-adsorption in the case of **Cu_2Br_2**-[**O,O**].
(56) Nakamoto, K. *Infrared and Raman Spectra of Inorganic and Coordination Compounds*, 6th ed.; Wiley: Hoboken, NJ, 2009; Part B, pp p107−110.
(57) Kitching, W.; Moore, C. J.; Doddrell, D. *Inorg. Chem.* **1970**, *9*, 541−549.
(58) Langs, D. A.; Hare, C. R.; Little, R. G. *Chem. Commun.* **1967**, 1080−1081.
(59) Chandrasekaran, P.; Mague, J. T.; Balakrishna, M. S. *Inorg. Chem.* **2006**, *45*, 6678−6683.